Journal of Sound and Vibration (2001) **243**(2), 241–268
doi:10.1006/jsvi.2000.3342, available online at http://www.idealibrary.com on IDEAL®

FLOW-INDUCED VIBRATION OF AN EULER–BERNOULLI BEAM

X. Q. Wang, R. M. C. So and Y. Liu

Department of Mechanical Engineering, The Hong Kong Polytechnic University, Hung Hom, Kowloon, Hong Kong. E-mail: mmgwang@polyu.edu.hk

(*Received* 27 *January* 2000, *and in final form* 11 *July* 2000)

Flow-induced vibration of a fixed–fixed elastic cylinder with a large aspect ratio (≈ 58) is considered. The structural vibration is modelled by the Euler–Bernoulli beam theory, and the normal mode method is used to analyze the structural response. The flow field are resolved using a finite element method and the flow-induced forces are thereby calculated. Altogether two different cases are examined, one at resonance and another at off-resonance. Results thus obtained are compared with experimental measurements and a discrete-parameter model [a two-degree-of-freedom (2-d.o.f.) model] analysis. The comparison shows that, while the 2-d.o.f. model gives reasonable prediction of the mid-span vibration displacements for the resonant and off-resonant case, the present method yields the span-wise multi-mode response of the cylinder similar to that observed experimentally. Based on these results, a correction formula is derived to estimate the span-wise vibration from the 2-d.o.f. model result. Correlation results are also presented to show that fluid–structure interactions mainly affect the phase relation between the fluid forces and the corresponding vibration of the cylinder. Such influences have different effects along the cylinder span.

1. INTRODUCTION

A simple flow-induced vibration problem is one represented by a two-dimensional cylinder in a cross-flow. In this problem, two different situations can be identified: One is the free vibration of the cylinder given rise by the flow-induced forces created by the shed vortices, another is the forced vibration of the cylinder. The forcing can be mechanically applied [1, 2], or it can be induced by upstream vortices [3]. In the forced vibration case, if the cylinder is also elastic, there will be vortex-induced vibrations superposed on the forced vibration. For a relatively rigid cylinder, the problem is dominated by the imposed oscillation frequency. A lock-on phenomenon arises when the forcing frequency is equal to the shedding frequency [1, 2, 4]. On the other hand, in the free-vibration case, where there is no external excitation, the phenomenon of interest is resonance (or synchronization). This occurs when the shedding frequency is identical to the natural frequency of the combined fluid–cylinder system [5–7]. The present study only considers the free-vibration case and leaves the forced-vibration case to a later investigation.

Flow-induced vibration of a single circular cylinder has been extensively investigated [4, 8, 9]. Usually, a cylinder with large aspect ratio and no end exposed in the flow is considered, so that the flow is essentially two-dimensional along a major portion of the span. However, the structural response is not necessarily two-dimensional when the cylinder is elastic. Among the experimental investigations are the studies of references [10–15], to mention a few. On the other hand, relatively little work has been carried out on

0022-460X/01/220241 + 28 $35.00/0

the numerical simulation of flow-induced vibration of a cylinder in a cross-flow. In some earlier work, only the transverse vibration of the cylinder, which was assumed to be harmonic, was considered [16]. The motion of the cylinder was restricted to one degree of freedom. It is worth noting that the one-degree-of-freedom (1-d.o.f.) structural model was also adopted, along with a Van der Pol-type equation for the lift force, to give a semi-analytical analysis of the vortex-induced resonant vibration of an elastically mounted rigid cylinder [5, 17, 18]. In a different numerical approach, Zhou *et al.* [19] studied the resonance behavior at a Reynolds number, $\mathrm{Re} = 200$, using a two-degree-of-freedom (2-d.o.f.) model to account for the structural response in both the transverse and stream-wise direction and a vortex dynamics method to resolve the flow field. It was found that a 1-d.o.f. model might not be sufficient to describe the structural dynamics correctly since the stream-wise motion of the cylinder does affect the transverse motion. The 2-d.o.f. model was also used by So *et al.* [20] to simulate vortex-induced vibration of a cylinder at sub-critical Re. Instead of the vortex dynamics method, a finite element technique was used to solve the two-dimensional Navier–Stokes equation governing the flow field. The numerical results were compared with experimental measurements at the mid-span of an elastic cylinder, and reasonable agreement was obtained. In all these calculations, the vibration modes and the span-wise correlation of the vibration amplitude with the flow-induced forces are not known, because the 2-d.o.f. model cannot provide such information.

A distributed-parameter beam model is thus necessary. Numerous investigators [21–23] used such a model to examine the flexural vibration of an elastic cylinder. Assuming the Euler–Bernoulli beam model, Skop and Griffin [24] and Skop and Balasubramanian [25] extended the semi-analytical approach to treat elastic cylinders. Mukhopadhyay and Dugungji [26] also invoked this approach to study wind-excited vibration of a square cantilever beam. However, the use of distributed-parameter beam model in numerical simulations has not been attempted so far. In a direct numerical simulation of the flow past a vibrating cable, Newman and Karniadakis [27] expressed the structural motion as a Fourier expansion along the cable span. This is equivalent to using the distributed-parameter string model for the cable without considering the boundary conditions, that is, the cable is assumed to be infinitely long.

Usually, experimental studies were carried out with finite-span cylinders having fairly large aspect ratios and the cylinders were fixed at both ends. Thus, the vortex-induced motion would be the superposition of different mode responses depending on whether the case under investigation is off-resonance or not, and whether the flow is three dimensional or not. In practice, especially for $Re > 400$, the wake flow is not two dimensional [28]; hence the induced force along the span is not constant. None of the above approaches could be easily modified to simulate the actual experimental conditions; therefore, span-wise vibration and modal information of the cylinder are not available. Also, the approaches were not suitable for problems where the non-linear fluid–structure interaction becomes very dominant, such as in resonance or close to resonance situation [29]. In view of this, the present objective is to concentrate on the modal analysis of the fluid–cylinder system and attempt to simulate the experimental investigations directly assuming two-dimensional laminar flow.

If modal analysis is used to determine the cylinder vibration, then a three-dimensional flow calculation program has to be used to analyze the flow if the fluid structure interaction were to be predicted correctly. Therefore, the assumption of two-dimensional laminar flow needs justification. This is especially true for flows whose $Re > 1000$, because recent numerical studies [30, 31] have shown that the wake flow is three-dimensional and turbulent even when the approach flow is laminar and two-dimensional. In

flow-induced vibration problems, the important parameters to replicate are the frequencies of vortex shedding and the amplitude of oscillations of the unsteady forces. If these two parameters are calculated fairly correctly under the two-dimensional assumption, the structural dynamics could be estimated correctly as well, and the possibility of resolving resonance behavior could be much enhanced.

In the subcritical Re range, the mean drag is fairly constant and so is the Strouhal number [32–34]. Furthermore, in this Re range, if the oncoming flow is uniform and laminar, Strouhal excitation still dominates and the cylinder response is Strouhal-like up to $Re > 10^5$ [35]. This suggests that a laminar formulation to the flow-induced vibration problem in this Re range could be appropriate as long as the induced force is Strouhal excitation and its major frequency is identical to the vortex shedding frequency. So *et al.* [20] used these arguments to justify the two-dimensional laminar approach for long slender cylinders with $Re < 5000$. Good agreement with experimental data has been obtained for rigid and elastic cylinders in a cross flow. In view of this, their two-dimensional laminar flow analysis will be used in the current investigation.

Therefore, the present objective is to introduce the normal mode method into the numerical simulation, with the aim of investigating the free vibration of a slender elastic cylinder with fixed ends in a cross flow. The flow field is still simulated by the finite element method of So *et al.* [20], but the Euler-Bernouilli beam theory is used to model the flexural vibration of the cylinder, and the normal mode method is used to determine the span-wise structural response in the lift and drag direction. In this formulation, the fluid-structure interaction is taken into account directly through the time marching technique proposed by Jadic *et al.* [36]. A comparison with experimental measurements and the numerical results obtained from the 2 d.o.f. model is carried out. Based on these calculations, a correction formula for the 2 d.o.f. model is derived to estimate the cylinder span-wise vibration. The results are compared with experimental data obtained for the resonant and off-resonant cases.

2. NUMERICAL FORMULATION

There are four components to the numerical formulation of any fluid–structure interaction problem if it is to be evaluated correctly. The first concerns with the modelling of the flow field around the structure. This model should be versatile enough to accommodate a moving boundary in order to allow for the motion of the structure. The second is the evaluation of the dynamics of the structure as a result of the flow-induced forces. If this model is to be complete, it should be able to resolve the vibrations of the structure taking into account numerous effects associated with the structural properties and the mode shape. The third is the ability to resolve the fluid–structure interaction accurately, so that at any time step the unsteady fluid forces acting on the structure are correctly determined and the motions of the structure are calculated with reliability. Finally, it is the analysis of the calculated results. All calculated properties, such as the velocities, the lift and drag coefficients, the displacement amplitudes, etc., are in the form of time series. In principle, the time series contain all the information concerning the behavior of the flow, fluid damping and the structural dynamics. The key is to find a data analysis technique that could extract the information out completely with accuracy.

The time-marching method proposed by Jadic *et al.* [36] addresses these four components in a fairly complete manner. The present formulation intends to improve on their proposal in two ways. The first is to use a general numerical method to calculate the flow and the wake behind the structure in order to relax the free wake model, which is only appropriate for attached flows. The finite element method with a moving mesh proposed by

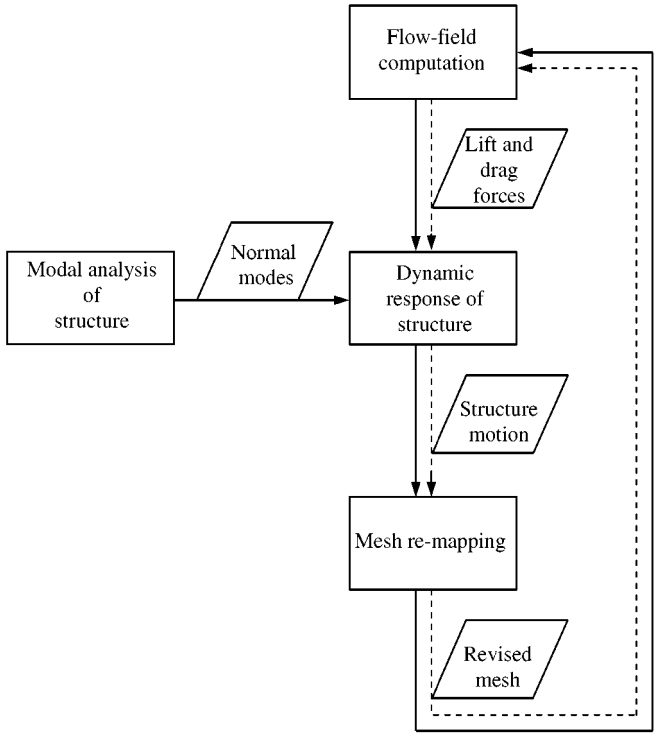

Figure 1. The flow chart illustrating the principle of the time-marching technique.

So *et al.* [20] is adopted. The second is to use the Euler–Bernoulli beam model for the structural dynamics, thus replacing the 2-d.o.f. model used in references [20, 36]. The flow chart illustrating the principle of the time-marching technique is shown in Figure 1.

In the present problem, the cylinder motion at any time step is completely controlled by the fluid forces, which are determined by the flow around the cylinder at that time step. The cylinder motion is, in turn, used to modify the boundary conditions of the flow field, from which the fluid forces are updated and used to calculate the cylinder motion at the next time step. This is where the moving mesh concept can be used to treat the moving boundary problem. Instead of using the Lagrangian–Eulerian method [37], an alternative mesh re-mapping procedure [20, 38] is invoked. This procedure can be easily implemented into the operator-splitting method, which is used to resolve the flow field in the present approach.

2.1. THE FLUID FLOW MODEL

A two-dimensional flow of an incompressible, viscous Newtonian fluid around an elastic slender cylinder fixed at both ends is considered. The flow is governed by the Navier–Stokes equations

$$\frac{\partial \mathbf{u}}{\partial t^*} + (\mathbf{u}\cdot\nabla)\mathbf{u} = -\nabla p + \frac{1}{\mathrm{Re}}\nabla^2\mathbf{u}, \qquad \nabla\cdot\mathbf{u} = 0, \tag{1,2}$$

where $\mathbf{u}$ is the dimensionless velocity vector normalized by the free-stream velocity U_∞, $t^* = tU_\infty/D$ is the dimensionless time, p is the dimensionless pressure normalized by ρU_∞^2,

$\mathrm{Re} = U_\infty D/v$ is the Reynolds number, D is cylinder diameter, ρ is fluid density and v is the fluid kinematic viscosity. The boundary and initial conditions can be specified as

$$\mathbf{u}|_S = \mathbf{u}_b \quad \text{and} \quad \mathbf{u}|_{t=0} = \mathbf{u}_0, \tag{3}$$

where S is the boundary of the domain V occupied by the fluid.

The operator-splitting method [39] is used to solve the Navier–Stokes equations. The θ scheme of the operator-splitting method is invoked for time discretization, thus de-coupling the non-linear equations into the following three fractional time steps:

$$\textit{Step 1:} \quad \frac{\mathbf{u}^{n+\theta} - \mathbf{u}^n}{\theta \Delta t^*} - \alpha v \nabla^2 \mathbf{u}^{n+\theta} + \nabla p^{n+\theta} = \beta v \nabla^2 \mathbf{u}^n - (\mathbf{u}^n \cdot \nabla)\mathbf{u}^n,$$

$$\nabla \cdot \mathbf{u}^{n+\theta} = 0, \tag{4a}$$

$$\textit{Step 2:} \quad \frac{\mathbf{u}^{n+1-\theta} - \mathbf{u}^{n+\theta}}{(1-2\theta)\Delta t^*} - \beta v \nabla^2 \mathbf{u}^{n+1-\theta} + (\mathbf{u}^{n+1-\theta} \cdot \nabla)\mathbf{u}^{n+1-\theta} = \alpha v \nabla^2 \mathbf{u}^{n+\theta} - \nabla p^{n+\theta}, \tag{4b}$$

$$\textit{Step 3:} \quad \frac{\mathbf{u}^{n+1} - \mathbf{u}^{n+1-\theta}}{\theta \Delta t^*} - \alpha v \nabla^2 \mathbf{u}^{n+1} + \nabla p^{n+1} = \beta v \nabla^2 \mathbf{u}^{n+1-\theta} - (\mathbf{u}^{n+1-\theta} \cdot \nabla)\mathbf{u}^{n+1-\theta},$$

$$\nabla \cdot \mathbf{u}^{n+1} = 0, \tag{4c}$$

where Δt^* is the time step, θ is a number between 0 and 0·5, $\alpha = (1-2\theta)/(1-\theta)$ and $\beta = \theta/(1-\theta)$. After time discretization, the equations for the first and the third steps are of the Stokes type, while the equation for the second step is of the advection type. At each fractional time step, the spatial discretization is carried out using the standard Galerkin method.

After the velocity and the pressure field has been obtained, the force applied to the structure is calculated using the following formula:

$$\mathbf{f}(z^*, t^*) = \oint\!\!\int \left(-p\mathbf{n} + \frac{1}{\mathrm{Re}} (\nabla \mathbf{u} + \nabla \mathbf{u}^{\mathrm{T}}) \cdot \mathbf{n} \right) \Delta z \, \mathrm{d}s, \tag{5}$$

where the integration is performed around the circumference of the cylinder with arc length s at each span-wise location z^*, Δz is the elemental length along the span and $\mathbf{n}$ is the outward unit normal on the cylinder. The force vector, $\mathbf{f} = \{f_D \; f_L\}$, consists of two components, the dimensionless unsteady drag and lift force. Thus, the lift and drag coefficients are defined as $C_L = 2f_L/(\rho U_\infty^2 \Delta z \pi D)$ and $C_D = 2f_D/(\rho U_\infty^2 \Delta z \pi D)$ respectively. All the calculated results are in the form of time series. From this point on, an overbar is used to denote the time average and a prime to designate the root-mean-square (r.m.s) value of the signal. Therefore, the mean and r.m.s. value of C_D is $\bar{C}_D$ and C_D' respectively.

2.2. THE STRUCTURAL DYNAMICS MODEL

The modal analysis method is proposed for the present analysis and the vibration of the cylinder is modelled by the Euler–Bernoulli beam theory [40]. According to this theory, the dimensional equation of motion of the cylinder is given by

$$m_{cy} \frac{\partial^2 \mathbf{w}(z,t)}{\partial t^2} + c \frac{\partial \mathbf{w}(z,t)}{\partial t} + EI \frac{\partial^4 \mathbf{w}(z,t)}{\partial z^4} = \mathbf{F}(z,t). \tag{6}$$

When the cylinder is fixed at both ends, the boundary conditions can be specified as

$$\mathbf{w}(-L/2, t) = 0, \quad \mathbf{w}(L/2, t) = 0, \quad \frac{\partial \mathbf{w}(-L/2, t)}{\partial z} = 0, \quad \frac{\partial \mathbf{w}(L/2, t)}{\partial z} = 0, \tag{7}$$

where $\mathbf{w} = \{X\ Y\}$ is the displacement vector consisting of the displacement components in the drag(x) and lift (y) direction, L is the length of the cylinder, EI is the stiffness, m_{cy} and c are the mass and damping coefficient per unit length of the cylinder, respectively, and $\mathbf{F} = \{F_D,\ F_L\}$ is the fluid force vector. The material of the cylinder is assumed to be isotropic and homogeneous, and the structural coupling between the motion in the x and y directions is not considered.

Using the modal analysis method, the solution of equation (6) can be assumed in the form

$$\mathbf{w}(z, t) = \sum_{m=1}^{N} W_m(z)\boldsymbol{\eta}_m(t), \tag{8}$$

where $W_m(z)$ is the mth normal mode shape of the undamped cylinder associated with the natural frequency f_{nm}, $\boldsymbol{\eta}_m$ is the generalized co-ordinate, and N is the number of normal modes considered. Applying the normal mode method, the following dynamic equation can be deduced:

$$\ddot{\boldsymbol{\eta}}_m \to 2\zeta_{sm}(2\pi f_{nm})\dot{\boldsymbol{\eta}}_m + (2\pi f_{nm})^2 \boldsymbol{\eta}_m = \frac{\mathbf{F}_m}{m_{cy}}. \tag{9}$$

Here, ζ_{sm} is the mth mode damping ratio of the cylinder and the dot represents time derivative. The dynamic equation (9) is made dimensionless using the same parameters as those adopted for the Navier–Stokes equations, thus giving rise to

$$\ddot{\boldsymbol{\eta}}_m + 2\zeta_{sm}\left(\frac{2\pi}{U_{rm}}\right)\dot{\boldsymbol{\eta}}_{nm} + \left(\frac{2\pi}{U_{rm}}\right)^2 \boldsymbol{\eta}_m = \frac{\mathbf{f}_m}{M_r}, \tag{10}$$

where $U_{rm} = U_\infty / f_{nm} D$ is the reduced velocity corresponding to f_{nm}, $M_r = m_{cy}/\rho D^2$ is the mass ratio, and $\mathbf{f}_m$ is the mth mode generalized dimensionless force given by

$$\mathbf{f}_m(t^*) = \int W_m(z^*)\mathbf{f}(z^*, t^*)\,\mathrm{d}z^*, \quad m = 1, 2, \ldots . \tag{11}$$

The present beam model predicts both the transverse and the stream-wise vibration of the cylinder along the span. In this sense, it accounts for the three-dimensional structural dynamics. The unsteady force vector, $\mathbf{f} = \{f_D, f_L\}$, is generally a function of time and the span-wise co-ordinate and, in principle, should be calculated based on a three-dimensional flow model. However, the flow field is assumed to be two-dimensional for a long slender cylinder, that is, $\mathbf{f}$ is independent of the span-wise co-ordinate z^*. Thus, the generalized force can be expressed as

$$\mathbf{f}_m(t^*) = \int W_m(z^*)\mathbf{f}(t^*)\,\mathrm{d}z^*, \quad m = 1, 2, \ldots . \tag{12}$$

A fourth order Runge–Kutta method is used to solve equation (10). Once $\boldsymbol{\eta}_m(t^*)$ and $\dot{\boldsymbol{\eta}}_m(t^*)$ are evaluated, the dimensionless displacement and velocity of the cylinder are

calculated using the following equations:

$$\mathbf{w}^*(z^*, t^*) = \sum_{m=1}^{N} W_m(z^*)\boldsymbol{\eta}_m(t^*), \qquad \dot{\mathbf{w}}^*(z^*, t^*) = \sum_{m=1}^{N} W_m(z^*)\dot{\boldsymbol{\eta}}_m(t^*). \tag{13a, b}$$

2.3. CORRECTION FORMULA FOR 2-d.o.f. MODEL

The 2-d.o.f. model is often used in previous numerical investigations of vortex-induced vibration, where only one vibration mode (usually the fundamental mode) is considered. The dynamic equation for the 2-d.o.f. model, in dimensionless form, can be written as

$$\ddot{\mathbf{w}}(t^*) + 2\zeta_s\left(\frac{2\pi}{U_r}\right)\dot{\mathbf{w}}(t^*) + \left(\frac{2\pi}{U_r}\right)^2 \mathbf{w}(t^*) = \frac{\mathbf{f}(t^*)}{M_r}, \tag{14}$$

where ζ_s is the damping ratio of the cylinder which is assumed to be constant, $U_r = U_\infty / f_n^* D$ is the reduced velocity, f_n^* is the natural frequency of the stationary cylinder and $\mathbf{f}(t^*)$ is the unsteady fluid force vector. In order to compare the beam model with the 2-d.o.f. model, equation (10) is re-written in the form

$$W_m(z^*)\ddot{\boldsymbol{\eta}}_m(t^*) + 2\zeta_{sm}\left(\frac{2\pi}{U_{rm}}\right)W_m(z^*)\dot{\boldsymbol{\eta}}_m(t^*) + \left(\frac{2\pi}{U_{rm}}\right)^2 W_m(z^*)\boldsymbol{\eta}_m(t^*) = \frac{\mathbf{f}_m(t^*)\,W_m(z^*)}{M_r}, \tag{15a}$$

$$\ddot{\mathbf{w}}_m^*(z^*, t^*) + 2\zeta_{sm}\left(\frac{2\pi}{U_{rm}}\right)\dot{\mathbf{w}}_m^*(z^*, t^*) + \left(\frac{2\pi}{U_{rm}}\right)^2 \mathbf{w}_m^*(z^*, t^*) = \frac{\mathbf{f}(t^*)\,W_m(z^*)\int W_m(z^*)\,\mathrm{d}z^*}{M_r}, \tag{15b}$$

where m refers to the vibration mode considered in the 2-d.o.f. model. In general, the fluid force, $\mathbf{f}(t^*)$, in equations (14) and (15b) is not the same since the effect of the fluid–structure interaction might be different. However, from the numerical results to be presented later, it can be seen that the r.m.s. value and the dominant frequency of the fluid force is almost identical for the modal analysis method and the 2-d.o.f. model. Since the span-wise vibration shape represents the magnitude of the vibration only, such a feature makes it possible to estimate the span-wise vibration shape of the cylinder using the result obtained from the 2-d.o.f. model and the correction (15b). This is further discussed in section 3.1.

2.4. FLUID–STRUCTURE INTERACTION

From a computational point of view, flow-induced vibration is a moving boundary problem because the cylinder is free to move under the action of the flow-induced unsteady forces in the fluid. The boundary of the computational domain is varied with the cylinder motion, and the no-slip boundary condition is applied on the surface of the cylinder. The mesh is deformed accordingly also. The mesh re-mapping procedure proposed by Mooney and Stokes [38] is invoked in the present approach. A Laplacian equation of displacement is solved to minimize the local mesh deformation. The Laplacian equation is expressed as

$$\nabla^2 \boldsymbol{\delta} = 0 \tag{16}$$

with the boundary conditions given by $\boldsymbol{\delta} = 0$ at the outer boundary and $\boldsymbol{\delta} = \mathbf{w}^*$ at the boundary of the cylinder where $\boldsymbol{\delta}$ is the deformation of the mesh nodes. The mesh is then

re-mapped according to the deformation. In order to correctly account for the fluid–structure interaction, a time marching is carried out within each time step in an iterative way, until the stable status is reached (Figure 1). In such a time-marching process, the cylinder motion, the flow field, and the fluid forces are updated but the time is not marching in reality. The dashed (virtual) line in Figure 1 shows this step in the numerical computation. The readers are referred to Jadic *et al.* [36] for a detailed description of the process.

2.5. DATA ANALYSIS

The time-marching approach gives time series for the fluid forces, cylinder vibrations, flow velocity profiles, and so on. Data analysis of these time series is necessary in order to obtain statistics and spectra, which add up to give an understanding of the flow-induced vibration problem. The computation of statistics is straightforward, while many methods are available for spectral analysis. One of them, the auto-regressive moving average (ARMA) method [41], has been successfully applied to perform spectral analysis of time series in both experimental and numerical studies of flow-induced vibration problems [15, 19, 20]. Therefore, this method is employed in the present study.

3. COMPARISON WITH MEASUREMENTS AND 2-D.O.F. PREDICTIONS

The free vibration of an elastic cylinder in a cross-flow at sub-critical Re range is simulated. The parameters of the fluid–structure system are chosen so that they match the experimental specifications [15] and are identical to the numerical cases considered by So *et al.* [20] in their 2-d.o.f. model calculations. That way, the present results can be compared with the experimental measurements and the 2-d.o.f. predictions.

The structural parameters of the cylinder are listed in Table 1. Two cases are chosen for comparison; one is the resonant case ($U_{r1} = 4{\cdot}5$, Re $= 994$), where the frequency of the first vibration mode of the fluid–cylinder system was found to be equal to the vortex-shedding frequency. The other is the off-resonant case ($U_{r1} = 16{\cdot}4$, Re $= 3900$), where no resonance or synchronization occurs. Here, U_{r1} is the reduced velocity corresponding to the natural frequency of the first mode of vibration of the cylinder. The spin-wise vibration of the cylinder is calculated using equations (13) and (15) at a series of span-wise locations, $z^* = 0$, 5·3030, 10·6061, 15·9091, 21·2121, 26·5152, and 29·1667, where $z^* = 0$ is the mid-span of the cylinder. Since the motion of the cylinder is assumed to be symmetric about the mid-span, only the vibration of one half of the cylinder needs to be calculated. The first four vibration modes of the cylinder are considered in the computation. Actually, since the mode shapes of

TABLE 1

Structural parameters of the cylinder

Material	L (mm)	D (mm)	M_r	Natural frequencies (Hz) and damping ratios (in stationary air)			
Acrylic	350·0	6·0	455·0	$f_{n1}^* = 99$ $\zeta_{s1} = 0{\cdot}03$	$f_{n2}^* = 272$ $\zeta_{s2} = 0{\cdot}02$	$f_{n3}^* = 534$ $\zeta_{s3} = 0{\cdot}017$	$f_{n4}^* = 883$ $\zeta_{s4} = 0{\cdot}01$

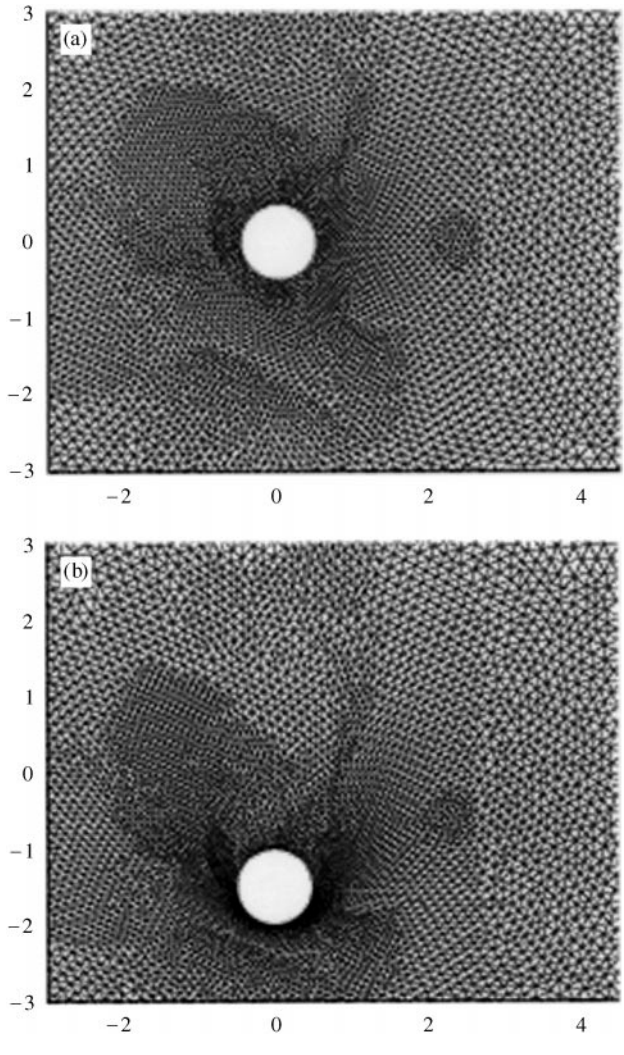

Figure 2. Illustration of the mesh deformation. Resonant case, $M_r = 1$: (a) undeformed mesh; (b) deformed mesh (at maximum displacement).

the second and the fourth modes are antisymmetric about the mid-span, the responses of these two modes are identically zero, thus only the first and third modes contribute to the the total vibration of the cylinder.

In order to illustrate the effectiveness of the mesh re-mapping technique, the finite element meshes at two different time steps for the resonant case are shown in Figure 2. This resonant case is identical to the case listed above, except that $M_r = 1$ has been assumed. The reason for this assumption is to obtain larger displacements so that the mesh deformation can be clearly shown. The finite element mesh at a time step when the cylinder has no displacement is shown in Figure 2(a). Its corresponding mesh at a time step when the cylinder reaches its maximum displacement is displayed in Figure 2(b). It is obvious that the mesh re-mapping technique is quite suitable for this kind of moving boundary problems.

3.1. OFF-RESONANT CASE

The time series of the calculated C_L, C_D, and X and Y displacements at the mid-span of the cylinder are plotted in Figures 3(a)–3(d) respectively. The dimensionless time step is 0·1. It can be seen that all time series have reached their stationary state, and the statistics given below are calculated based on the stationary period alone. The calculated Y'/D of the cylinder is plotted in Figure 4(a) for comparison with experimental measurements [15] and numerical results obtained from the 2-d.o.f. model. Again, the prime is used to denote r.m.s. value and the overbar to designate the time-average value. The comparison shows that the modal analysis calculations and the measurements give similar span-wise vibration shapes. Particularly, the multi-mode response of the cylinder is clearly reproduced by the modal analysis. The prediction by the 2-d.o.f. model is given in the figure by a dashed-dot line. It can be seen that the prediction is almost the same as that given by the modal analysis method at the mid-span of the cylinder.

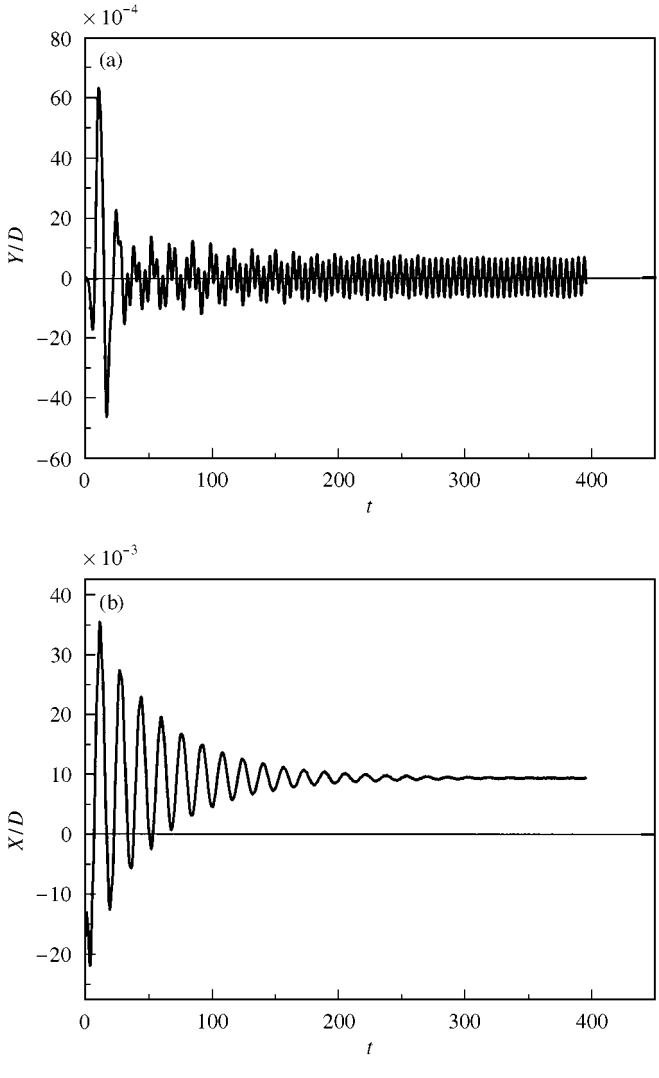

Figure 3. Time series of the fluid force coefficients and cylinder vibrations. Off-resonant case.

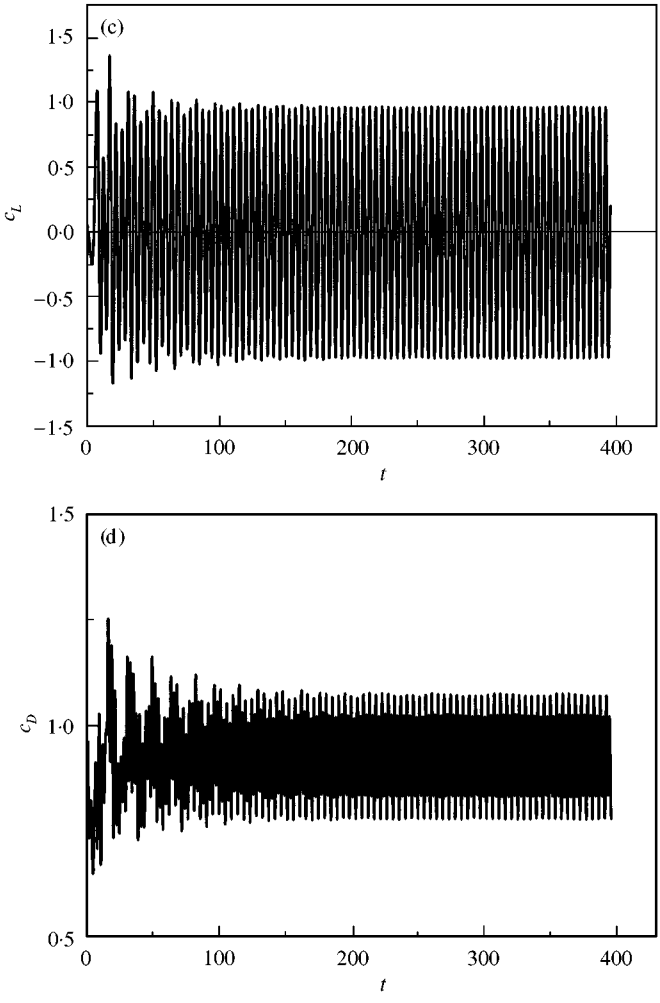

Figure 3. Continued.

The multi-mode response of the cylinder is the superposition result of the responses due to a number of vibration modes excited by the fluid force. The present method gives some detail on such a behavior (Figure 4(b)). The responses due to the first and the third mode (Modes 1 and 3) are plotted separately in the figure to show their own contributions. It can be seen that the amplitude ratio of Modes 1 and 3 is about 4 : 1, thus giving rise to the superposed behavior of the total vibration. It is slightly different for X'/D whose span-wise vibration shapes are shown in Figure 4(c). The stream-wise vibration consists of two components, one a static part and another a fluctuating part. Therefore, two span-wise vibration shapes are plotted, one is the purely fluctuating displacement (Figure 4(c)), and the other is the total motion including the static displacement (Figure 4(d)). It can be seen that the fluctuating span-wise vibration also shows the feature of the multi-mode response, while the span-wise vibration of the total motion does not, because the static displacement is dominant and has a shape similar to the response of Mode 1.

The normalized frequency spectra of Y/D at mid-span are compared in Figure 5. The values of the Strouhal number, St, the natural frequencies, f_{nm}, and the effective damping

ratios, ζ_{em}, are listed in Table 2, where m refers to the mode number and n denotes the natural frequency of the fluid–cylinder system. The effective damping ratio is the sum of the fluid damping and structural damping. It can be seen that the modal analysis method and the 2-d.o.f. model predicts the same value of St, and the prediction agrees well with experimental measurements, the relative error is about 6·7%. The present method predicts two natural frequencies of system, $f_{n1} = 0{\cdot}0728$, and $f_{n3} = 0{\cdot}3442$. They are in fair agreement with experimental measurements, where the peaks can be identified at $f_{n1} = 0{\cdot}0568$, and $f_{n3} = 0{\cdot}3029$. The 2-d.o.f. model predicts the first natural frequency at $f_n = 0{\cdot}0661$ only, since the third vibration mode is not considered. The predicted values of ζ_{em} by the present method and the 2-d.o.f. model are similar; both are larger than experimental measurements. This may be due to the fact that the initial values of the structural damping ratio given in Table 1 are calculated theoretically and slightly different from the actual experimental

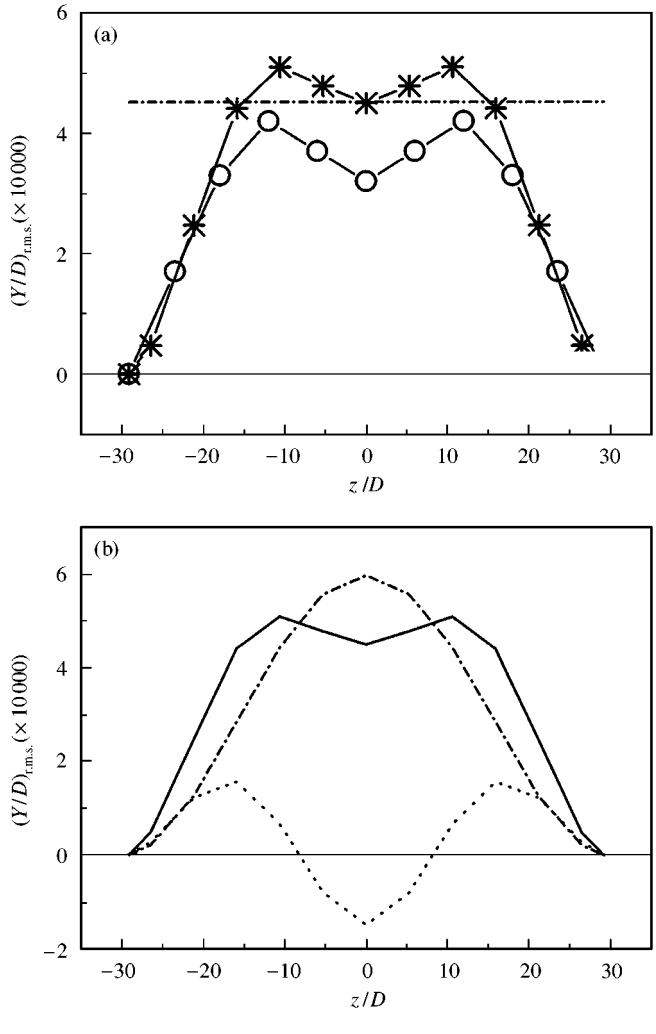

Figure 4. Span-wise vibration of the cylinder. Off-resonant case. (a) Comparison of computational and experimental results in the lift direction: —○—○—, experiment; —✳—✳—, computation (beam model); and - - · - · - ·, computation (2-d.o.f. model). (b) Calculated span-wise vibration of the cylinder in the lift direction: ——, total motion; - - · - · - ·, Mode 1; and · · · · ·, Mode 3. (c) Calculated span-wise vibration of the cylinder in the drag direction: ——, total motion; - - · - · - ·, Mode 1; and · · · · ·, Mode 3. (d) Calculated span-wise vibration of the cylinder in the drag direction: ——, total motion; - - · - · - ·, Mode 1; and · · · · ·, Mode 3.

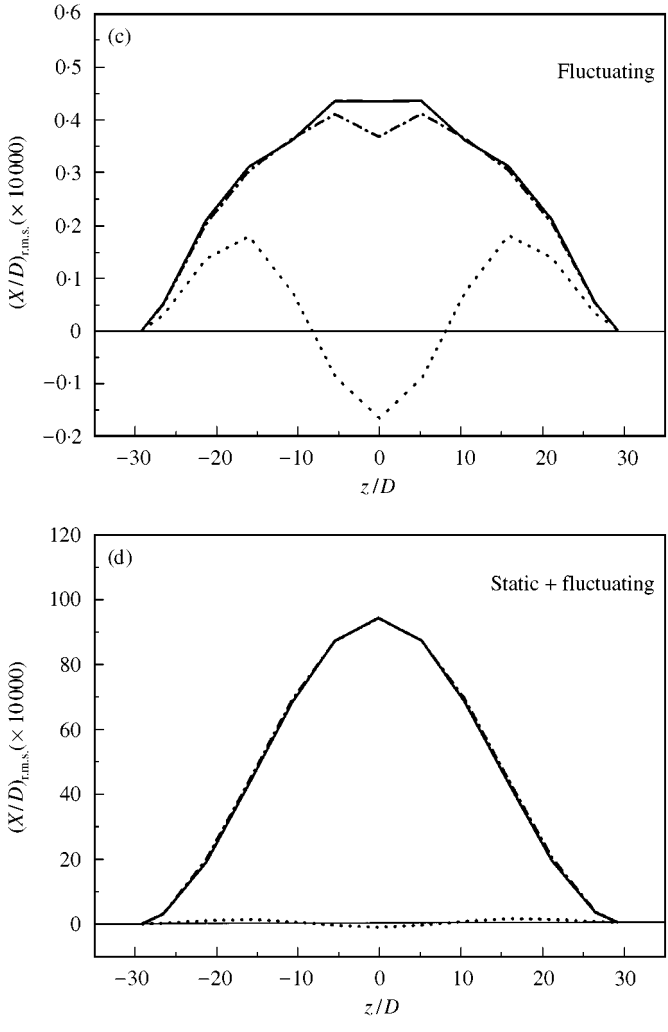

Figure 4. Continued.

values. Furthermore, during the experiments, the cylinder has to be mounted and dismounted regularly; thus the fixed-end support of the cylinder and hence the structural damping ratio might be affected.

Apart from the frequencies associated with Modes 1 and 3, more frequency peaks are observed in the experimental spectrum. The two peaks in the low-frequency range are associated with the fan and wind tunnel vibration. The peaks at $1/U_r \approx 0{\cdot}15$ and $0{\cdot}50$ are related to the second and the fourth mode of the cylinder respectively. Several factors in the experiment may contribute to the appearance of these two peaks, e.g., the cylinder (along with the end supports) is not perfectly uniform along the span or symmetric about its mid-span, the flow field is not perfectly two dimensional, or the presence of flow turbulence.

A detailed comparison of the statistics at mid-span, obtained by experimental measurement, the modal analysis method, and the 2-d.o.f. model, is given in Table 3. It can be seen that the present approach and the 2-d.o.f. model give similar predictions of the lift and drag coefficients. At mid-span, the 2-d.o.f. model predicts the same Y'/D value as the present approach. However, considering the fact that the 2-d.o.f. model only takes the first mode of the cylinder into account, the 2-d.o.f. model prediction should be compared with

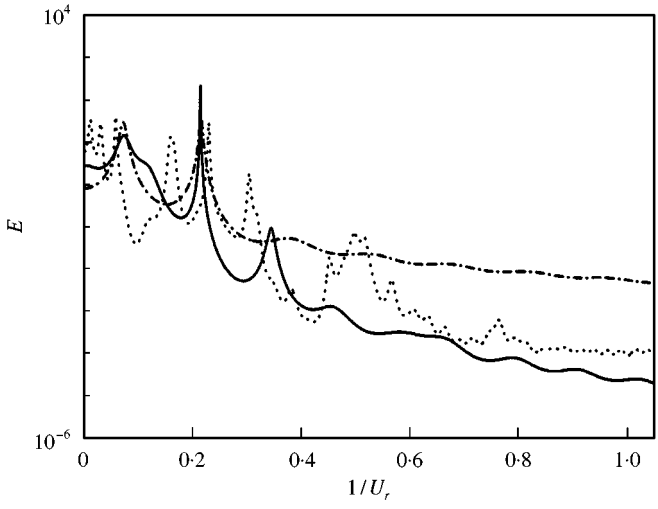

Figure 5. Comparison of frequency spectra of the cylinder vibration at mid-span: computation versus experiment. Off-resonant case: ——, computation (beam model); - - - - - - -, computation (2-d.o.f. model); and ·····, experiment.

TABLE 2

Comparison of Strouhal number, natural frequencies and damping ratios of the fluid–cylinder system in the off-resonant case ($U_{r1} = 16{\cdot}4$, Re = 3900)

	Experiment			Computation			
				2-d.o.f. model	Beam model		
	Total	Mode 1	Mode 3		Total	Mode 1	Mode 3
St	0·2284	—	—	0·2132	0·2132	—	—
f_{nm}	—	0·0568	0·3029	0·0661	—	0·0728	0·3442
ζ_{em}	—	0·0262	0·0078	0·1093	—	0·1675	0·0190

TABLE 3

Comparison of experimental and numerical results in the off-resonant case ($U_{r1} = 16{\cdot}4$, Re = 3900)

	Experiment			Computation			
				2-d.o.f. model	Beam model		
	Total	Mode 1	Mode 3		Total	Mode 1	Mode 3
$\bar{C}_L$	—	NA	NA	0·0018	− 0·0026	NA	NA
C'_L	—	NA	NA	0·6801	0·6783	NA	NA
$\bar{C}_D$	—	NA	NA	0·9362	0·9362	NA	NA
C'_D	—	NA	NA	0·0875	0·0888	NA	NA
$\bar{Y}/D$	0·0	—	—	0·00001	0·00002	0·00002	$-7{\cdot}2\times10^{-7}$
Y'/D	0·00032	—	—	0·00045	0·00045	0·00060	0·00015
$\bar{X}/D$	—	—	—	0·0070	0·0094	0·0093	0·0001
X'/D	—	—	—	$4{\cdot}16\times10^{-5}$	$4{\cdot}33\times10^{-5}$	$3{\cdot}66\times10^{-5}$	$1{\cdot}67\times10^{-5}$

the Y'/D value of Mode 1 predicted by the modal analysis method. It can then be seen that the modal analysis prediction is higher than the 2-d.o.f. result. This is not unexpected based on equations (13) and (14). When the predicted magnitude of the fluid force, $\mathbf{f}(t^*)$, is almost the same for the 2-d.o.f. model and the modal analysis method, the actual excitation forces are different by a factor of $W_n(z^*)\int W_n(z^*)\,\mathrm{d}z^*$ which is related to the normal mode of the cylinder. For the first mode, $W_n(z^*)\int W_n(z^*)\,\mathrm{d}z^* = 1{\cdot}3246$ at mid-span, and the excitation force given by the modal analysis method is larger, thus resulting in a larger prediction of Y'/D. The case is the same for $\bar{X}/D$ and X'/D.

3.2. RESONANT CASE

The time series of the calculated C_L, C_D, X and Y are plotted in Figures 6(a)–6(d) respectively. The time step used is identical to the off-resonant case, and again the

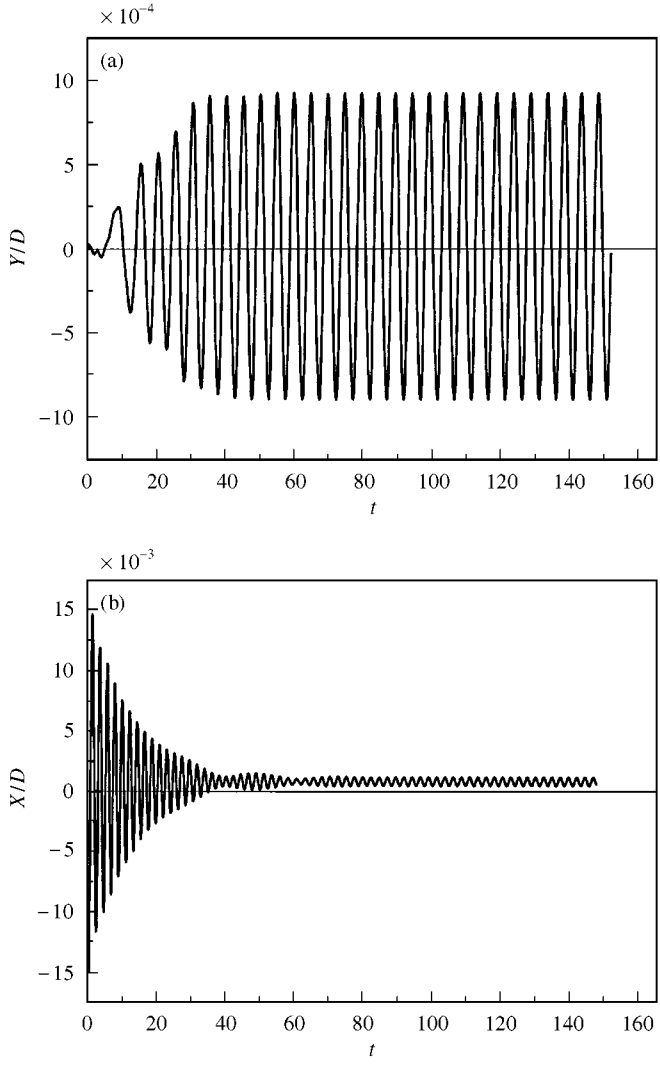

Figure 6. Time series of the fluid force coefficients and cylinder vibrations. Resonant case.

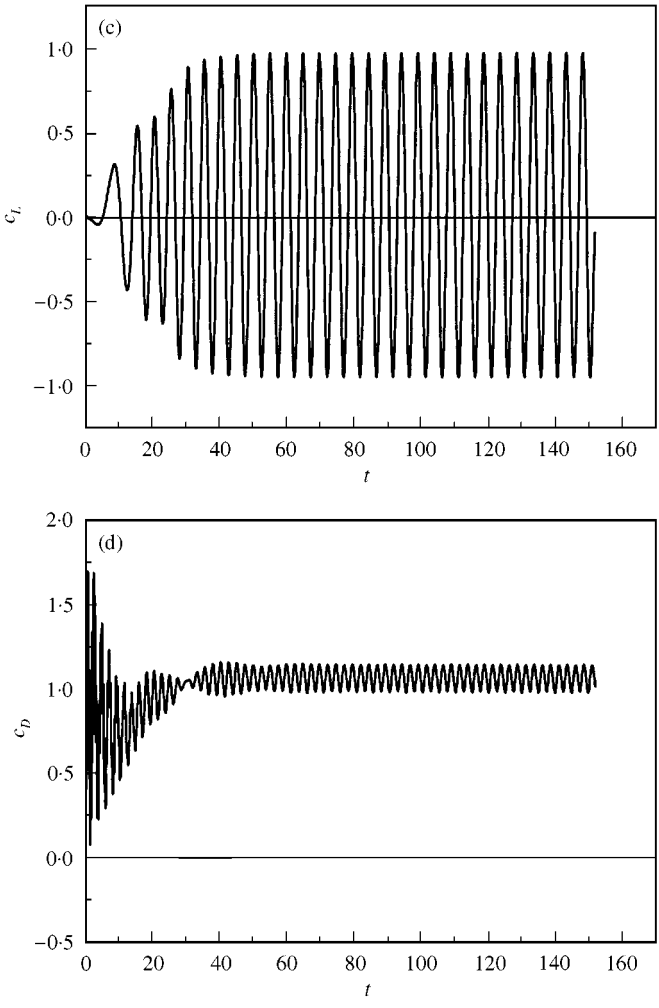

Figure 6. Continued.

calculation is carried out until a sufficiently long stationary period in these time series is available for analysis. Comparison of the span-wise distribution of Y'/D at resonance is given in Figure 7. The present method predicts the same vibration shape as the experimental measurement only in a qualitative sense. The quantitative agreement is poor compared to the off-resonant case. The 2-d.o.f. model result is also plotted in the figure, and it can be seen that it gives a slightly better estimate at mid-span. The difference between the 2-d.o.f. model calculation and the modal analysis result could be accounted for using the correction formula given in equation (15b); the analysis is given below. One possible reason for the big difference between calculations and measurements could be due to the fact that the reduced velocity at which the maximum resonance peak appears cannot be exactly located in the experiment. In fact, the resonance peak is identified at $U_{r1} = 4{\cdot}2$ experimentally, and the present numerical results are calculated at $U_{r1} = 4{\cdot}5$ since it is found that $U_{r1} = 4{\cdot}2$ is not the exact location where the resonance peak appears. Using $U_{r1} = 4{\cdot}2$ in the computation reduces the prediction of Y'/D, but two close peaks appear in the frequency spectrum,

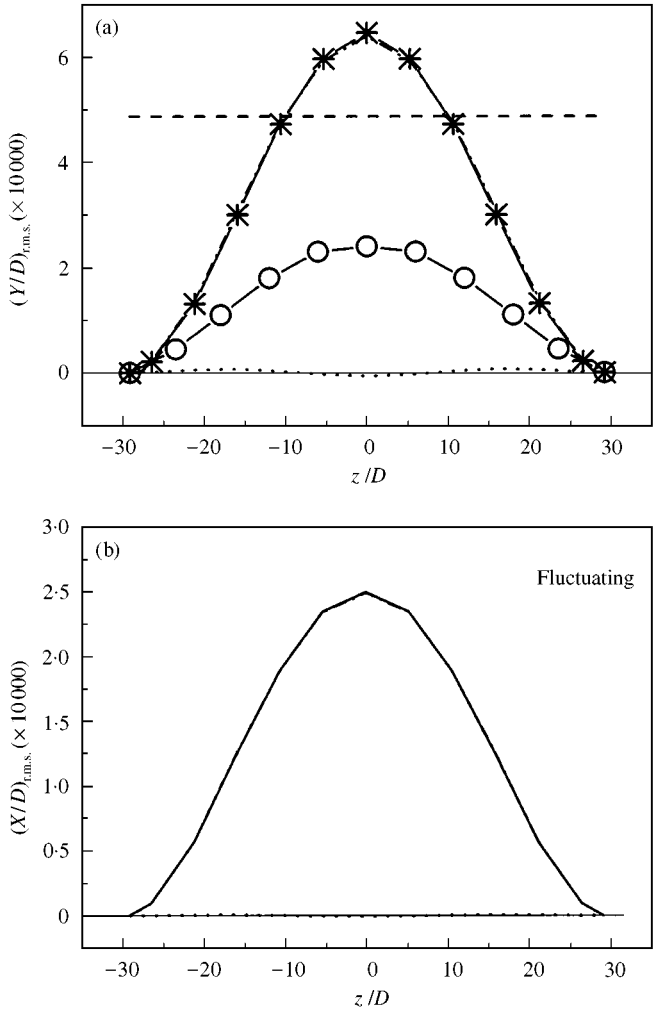

Figure 7. Span-wise vibration of the cylinder. Resonant case. (a) Comparison of computational and experimental results in the lift direction: —○—○—, experiment; —∗—∗—, computation (beam model, total motion), - - - - -, computation (2-d.o.f. model). Computation (beam model): · · · · ·, Mode 1; and - · - · - · -, Mode 3. (b) Calculated span-wise vibration of the cylinder in the drag direction: ——, total motion; - · - · - · -, Mode 1; and · · · · ·, Mode 3.

implying that the exact resonance point has not been reached yet. Another possible reason is the effects of three-dimensional flow. They affect flow-induced vibrations in two different ways. One is that the amplitude of the fluid force is not constant along the cylinder span, and the other is that the time-varying fluid force is not perfectly correlated along the span, and other is that the time-varying fluid force is not perfectly correlated along the span. A third possible reason is the acrylic cylinder used in the experiments. Since they are made from off-the-shelf acrylic tubes, the structural damping may show certain non-linearity when the vibration displacement is large, particularly in the resonant case. This also give rise to the lower displacement of the cylinder. A fourth reason could be the span-wise curvature of the cylinder, which results as a consequence of the mean drag acting on the cylinder. This differs from the planar assumption invoked in the Euler–Bernoulli beam

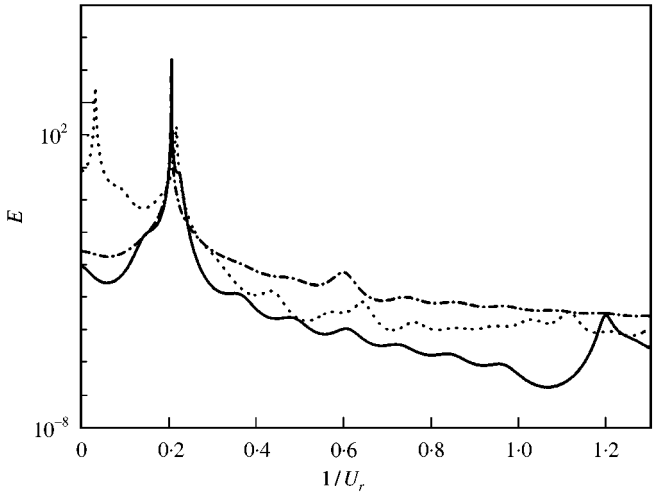

Figure 8. Comparison of frequency spectra of the cylinder vibration at mid-span: computation versus experiment. Resonant case: ——, computation (beam model); - - - - - -, computation (2-d.o.f. model); and ·····, experiment.

TABLE 4

Comparison of Strouhal number, natural frequencies and damping ratios of the fluid–cylinder system in the resonant case ($U_{r1} = 4{\cdot}5$, Re = 944)

	Experiment			Computation			
				2-d.o.f. model	Beam model		
	Total	Mode 1	Mode 3		Total	Mode 1	Mode 3
St	0·2150	NA	NA	0·2036	0·2036	NA	NA
f_{nm}	NA	0·2150	1·1255	0·2036	NA	0·2036	1·1971
ζ_{em}	NA	0·0104	0·0227	− 0·00008	NA	− 0·00032	0·0112

theory. At present, attempts are being made to evaluate the relative effects of these possible causes. The work will be reported separately later.

The response of the cylinder in the resonant case is also due to both Modes 1 and 3 (Figure 7(a)). Compared with the off-resonant case, however, the contribution of Mode 3 is almost zero, and the response of Mode 1 is dominant. The span-wise distribution of X'/D yields similar behavior (Figure 7(b)).

The comparison of the normalized frequency spectra of Y/D at mid-span is shown in Figure 8. The values of St, f_{nm} and ζ_{em} are listed in Table 4. At resonance, the shedding frequency, St, synchronizes with the fundamental natural frequency of the combined fluid–cylinder system, f_{n1}, and there is only one peak at $1/U_r = 0{\cdot}2036$ in the spectra of the numerical results. This agrees with the frequency peak at $1/U_r = 0{\cdot}2150$ in the experimental spectrum. The frequency peak at the low-frequency range ($1/U_r \approx 0{\cdot}02$) in the experimental

TABLE 5

Comparison of experimental and numerical results in the resonant case ($U_{r1} = 4{\cdot}5$, Re = 994)

	Experiment			Computation			
				2-d.o.f. model	Beam model		
	Total	Mode 1	Mode 3		Total	Mode 1	Mode 3
$\bar{C}_L$	—	NA	NA	$-0{\cdot}0010$	$-0{\cdot}0141$	NA	NA
C'_L	—	NA	NA	0·6861	0·6788	NA	NA
$\bar{C}_D$	—	NA	NA	1·0695	1·0684	NA	NA
C'_D	—	NA	NA	0·0623	0·0569	NA	NA
$\bar{Y}/D$	0·0	—	—	$-2{\cdot}8\times10^{-6}$	$-0{\cdot}00002$	$-0{\cdot}00002$	$1{\cdot}4\times10^{-7}$
Y'/D	0·00024	—	—	0·00049	0·00065	0·00064	0·00001
$\bar{X}/D$	—	—	—	0·00060	0·00081	0·00080	0·00001
X'/D	—	—	—	0·00021	0·00025	0·00025	$5{\cdot}6\times10^{-7}$

spectrum is due to low-frequency vibration of the wind tunnel. The present approach also predicts the response of the third mode of the fluid–cylinder system at $f_{n3} = 1{\cdot}1971$, while the experimental spectrum shows a peak at $f_{n3} = 1{\cdot}1255$. In the spectrum predicted by the 2-d.o.f. model, only the peak at $1/U_r = 0{\cdot}2036$ is observed. This is reasonable since the third mode of the cylinder is not considered in that model. The predicted ζ_{e3} by the present method is smaller than experimental measurement. The predictions of ζ_{e1} by both numerical methods are negative and very close to zero, indicating the appearance of a very sharp frequency peak where synchronization occurs.

The statistics of the experimental measurements, the modal calculations and the 2-d.o.f. model predictions are compared in Table 5. Both the present approach and the 2-d.o.f. model give similar predictions of the lift and drag coefficients. As for $\bar{Y}/D$, Y'/D, $\bar{X}/D$ and X'/D, the 2-d.o.f. model gives a relatively more accurate prediction, while the present approach predicts larger values. This discrepancy is analyzed below.

4. CORRECTION FOR THE 2-D.O.F. MODEL

In section 2.3, it is shown that the span-wise vibration shape can be estimated from the 2-d.o.f. model result, provided that the magnitude and the dominant frequency of the unsteady forces are not affected too much by the fluid–structure interaction. At mid-span, this condition is essentially verified by the statistics of C_L and C_D given in Tables 2 and 3. The span-wise distributions of C'_L and C'_D, and St, for both the resonant and off-resonant cases, are plotted in Figures 9(a)–9(b) respectively. It can be seen that they are almost constant along the cylinder span. This suggests that both the 2-d.o.f. model and the present approach predict similar magnitudes and dominant frequencies for the unsteady flow-induced forces.

A formula can then be derived to estimate the span-wise vibration of the cylinder from the 2-d.o.f. model result. This can be accomplished by dividing both sides of equation (15b) by $W_n(z^*)\int W_n(z^*)\,\mathrm{d}z^*$. Comparing with equation (14), the following result is obtained:

$$\mathbf{w}_n^*(z^*, t^*) = \mathbf{w}(t^*)\, W_n(z^*) \int W_n(z^*)\,\mathrm{d}z^*. \tag{17}$$

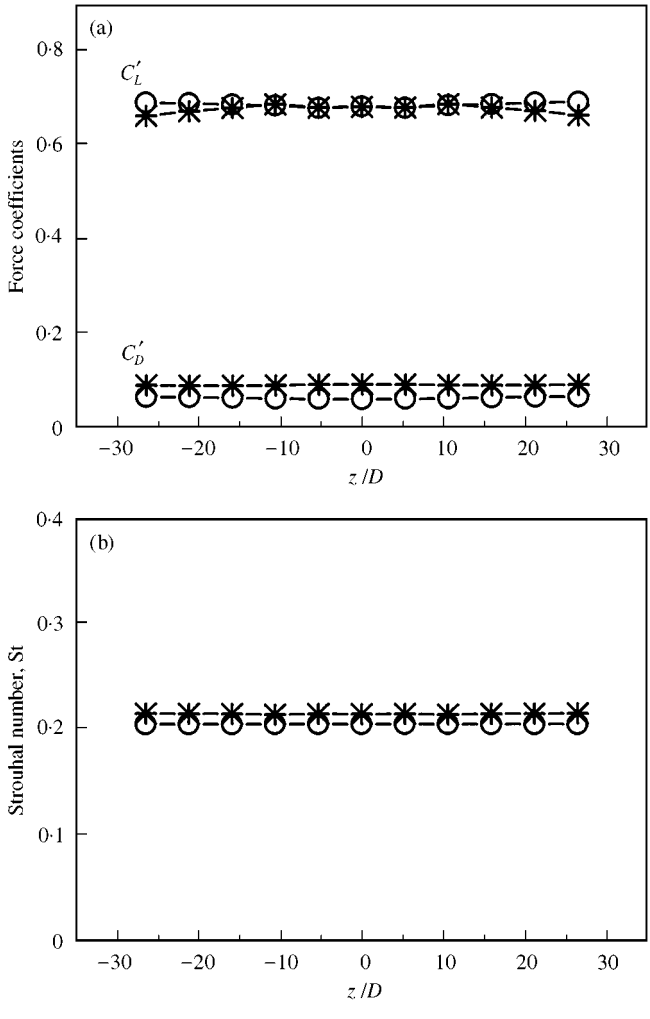

Figure 9. Span-wise force coefficients and Strouhal number. (a) Force coefficients: —✳—✳—, off-resonant case; —○—○—, resonant case. (b) Strouhal number: —✳—✳—, off-resonant case; —○—○—, resonant case.

The span-wise vibration shape estimated from the 2-d.o.f. model calculation using equation (17) is plotted in Figure 10 for comparison with the modal analysis result. It can be seen that the estimation is not too satisfactory for the off-resonant case (Figure 10(a)), but is very good for the resonant case (Figure 10(b)). This is expected because only one mode is considered in the 2-d.o.f. model. There is only one mode excited in the resonant case and both Modes 1 and 3 are excited in the off-resonant case. In the latter case, the span-wise vibration can be estimated using the vibration displacement at mid-span deduced from the modal analysis method. Equation (17) then becomes

$$\mathbf{w}_n^*(z^*, t^*) = \frac{\mathbf{w}_n^*(z_0^*, t^*)}{W_n(z_0^*)} W_n(z^*), \tag{18}$$

where $\mathbf{w}_n(z_0^*, t^*)$ is the vibration at $z^* = z_0^*$ obtained from the modal analysis method. The span-wise vibration calculated using equation (18) is plotted in Figure 11. It can be seen that

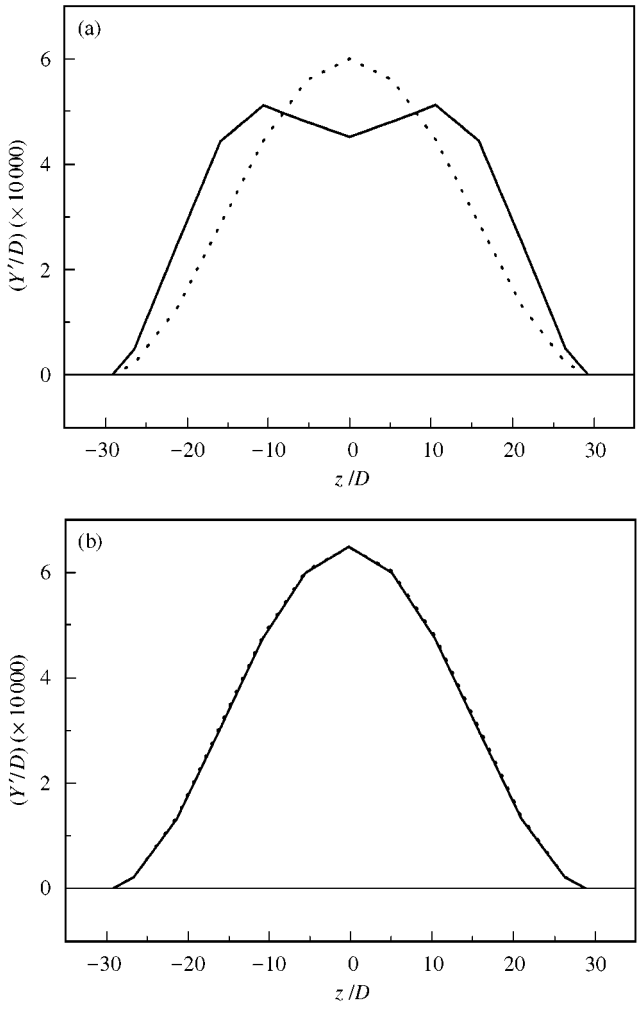

Figure 10. Span-wise vibration of the cylinder in the lift direction: comparison of the predictions by using the beam model and equation (20). (a) Off-resonant case; (b) Resonant case: ——, beam model; and · · · ·, equation (20).

the estimation is almost identical to the original result, at both off-resonance and resonance. Therefore, the difference between the 2-d.o.f. model results and the modal analysis calculations can be attributed to the effect of mode shape and can be accounted for by equation (15b).

5. FLUID–CYLINDER INTERACTION EFFECTS

Most studies of flow-induced vibration concentrate on the structural response and the flow-induced forces. Seldom attention was paid to the interaction phenomenon and the associated effective and fluid damping. Using ARMA, Zhou *et al.* [29] examined the effective damping associated with the free vibration of a single cylinder in a cross-flow. The method proposed by them has been used to deduce the effective damping ratio for the

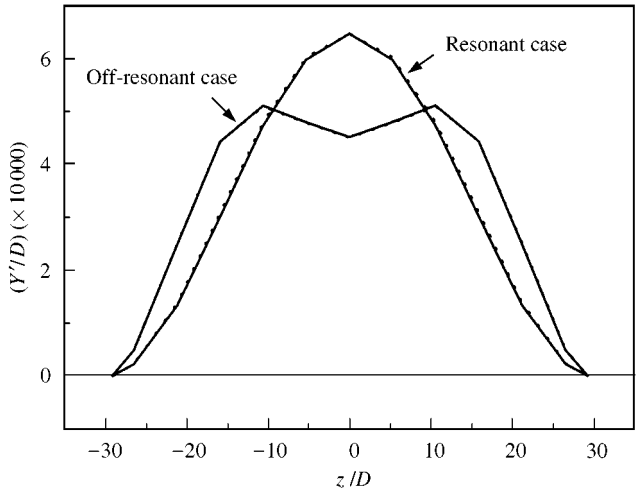

Figure 11. Span-wise vibration of the cylinder in the lift direction: comparison of the predictions by using the beam model and equation (21): ——, beam model; and ·····, equation (21).

different modes and reported in section 3.1. In this section, an attempt is made to evaluate the fluid–structure interaction. The present objective is not intended to study this problem extensively, however, some results are presented to help understand this important behavior.

5.1. FORCE–DISPLACEMENT CORRELATION

As can be seen from Figure 9, the span-wise distribution of C'_L, C'_D and St appear to be constant along the cylinder span, implying that the dominant frequencies and the magnitudes of the fluid forces are independent of the span-wise location. This is consistent with the finding of West and Apelt [14] based on experimental measurements at higher Re in the sub-critical range. The span-wise vibration amplitude of the cylinder is not constant, though. This implies that cylinder motion in the fluid–structure interaction phenomenon does not affect the r.m.s. magnitude and the dominant frequency of the fluid force significantly. However, it would be enlightening to further investigate the correlation between the force and the corresponding response, which is an indicator of the phase difference between them.

The correlation between two signals is defined as

$$\Lambda(P, Q) = E[(P - \mu_P)]E[(Q - \mu_Q)]/(\sigma_P \sigma_Q), \tag{19}$$

where P and Q are the time series of two signals, μ is the mean, and σ is the standard deviation of the signal. The correlation between the fluid forces and the corresponding cylinder displacements along the cylinder span is shown in Figure 12. First consider the correlation between C_L and Y/D. If fluid–structure interaction is not present, the correlation could be calculated by assuming that the fluid force is external to the structural vibration in equation (10). The results are $\Lambda(C_L, Y/D) = 0{\cdot}0035$ at resonance and $\Lambda(C_L, Y/D) = 0{\cdot}9989$ in the off-resonant case. When fluid–structure interaction is present, it

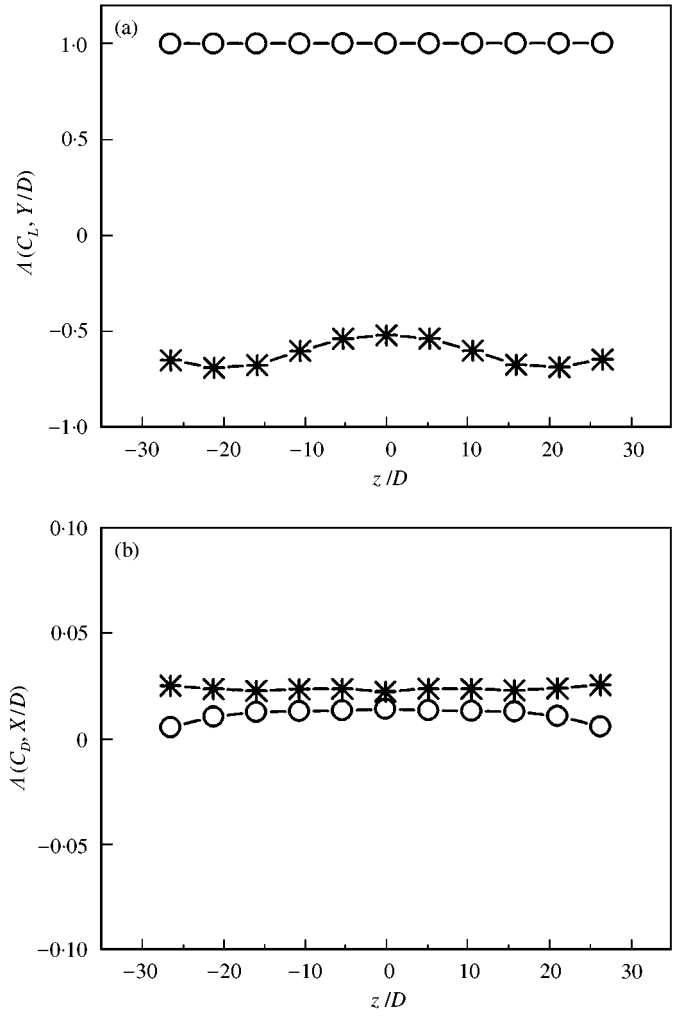

Figure 12. The correlation of the fluid force and corresponding displacement of the cylinder. (a) Transverse direction; (b) stream-wise direction: —✳—✳—, off-resonant case; —○—○—, resonant case.

can be seen that the phenomenon changes the correlation significantly. At resonance, $\Lambda(C_L, Y/D)$ is constant along the cylinder span and the value is around 0·9985. This indicates that, at resonance, the fluid–structure interaction synchronizes the fluid force and the cylinder vibration, not only in the frequency but also in the phase relation between them. Compared with the correlation when no interaction exists, $\Lambda(C_L, Y/D)$ changes from 0·0035 to 0·9985, that is, the phase difference between the force and the response is approximately $\pi/2$ shifted by the interaction. In the off-resonant case, $\Lambda(C_L, Y/D)$ shows a span-wise variation from $-0{\cdot}5242$ to $-0{\cdot}6513$, that is, the phase difference between the force and the displacement varies from $2\pi/3$, to $3\pi/4$, or $\pi/6$ to $\pi/4$ shifted by the interaction phenomenon. This suggests that the effects of the fluid–structure interaction on the phase interaction phenomenon. This suggests that the effects of the fluid–structure interaction on the phase difference vary along the span. The span-wise variation of the phase difference will be further discussed in the next section.

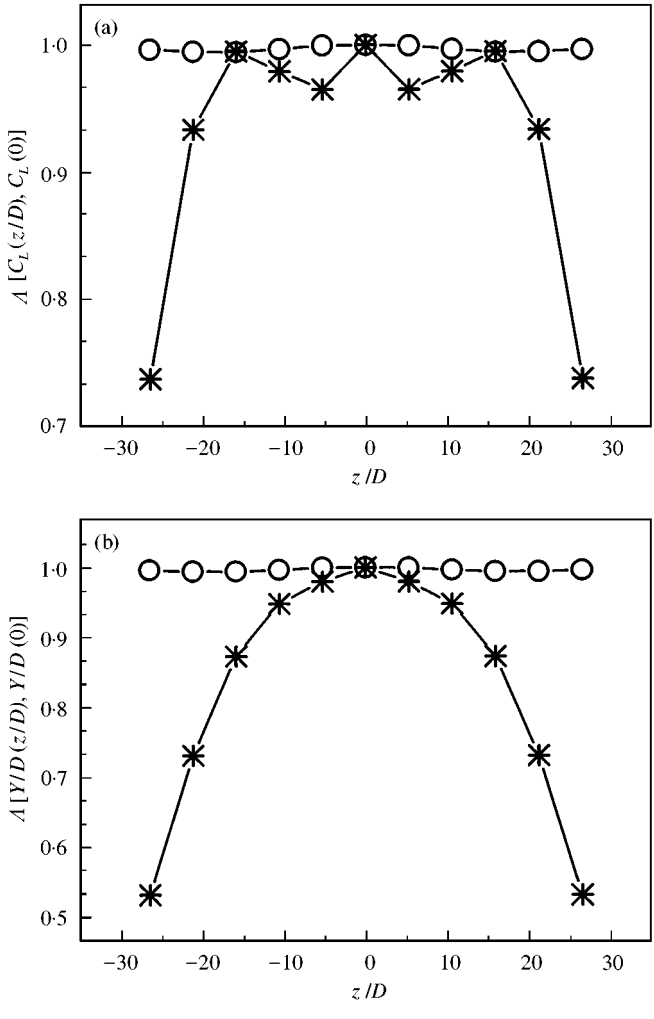

Figure 13. Span-wise correlation. (a) The fluid force; (b) the cylinder displacement: —✳—✳—, off-resonant case; —○—○—, resonant case.

In the drag direction, the correlation is close to unity when no interaction is assumed, i.e. $\Lambda(C_D, X/D) = 0{\cdot}9971$ at resonance and $\Lambda(C_D, X/D) = 0{\cdot}9974$ in the off-resonant case. When fluid–structure interaction is present, the correlation coefficient is close to zero; $\Lambda(C_D, X/D) = 0{\cdot}01$ at resonance and $\Lambda(C_D, X/D) = 0{\cdot}02$ in the off-resonant case and the phase difference is shifted by about $\pi/2$.

5.2. SPAN-WISE CORRELATION RESULTS

It is obvious from the above discussion that the correlation of the force and displacement in the lift direction shows a span-wise variation in the off-resonant case. In order to analyze this behavior further, the span-wise correlation of the fluid forces and the cylinder vibrations is examined. The span-wise correlation of a signal is defined as

$$\Lambda[P(z/D), P(0)] = E[(P(z/D) - \mu_{P(z/D)})]\,E[(P(0) - \mu_{P(0)})]/(\sigma_{P(Z/D)}\sigma_{P(0)}), \tag{20}$$

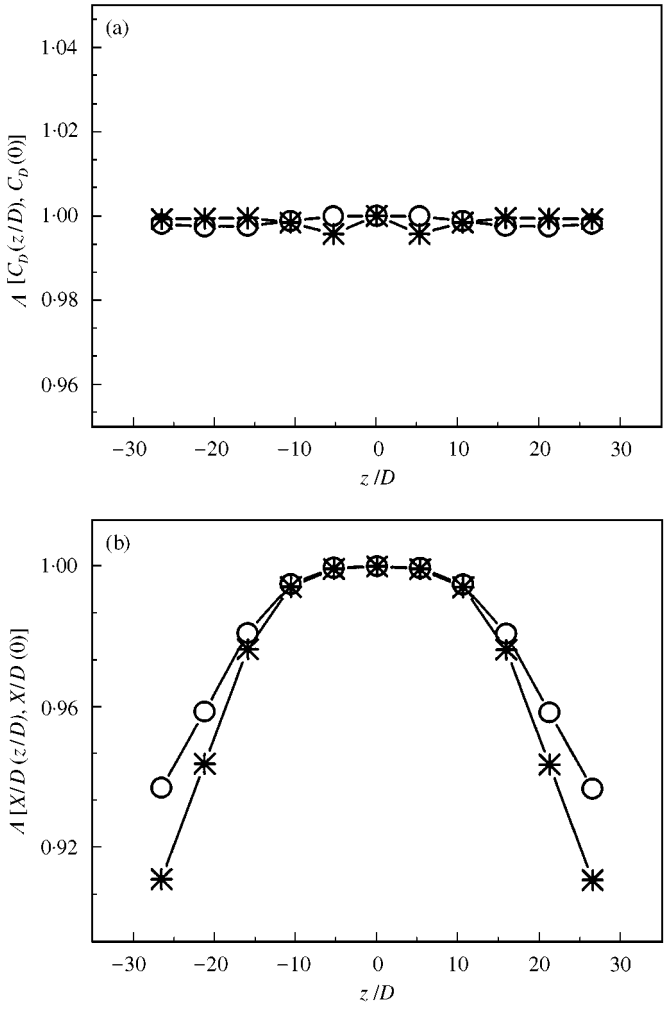

Figure 14. Span-wise correlation. (a) The fluid force; (b) the cylinder displacement: —✳—✳—, off-resonant case; —○—○—, resonant case.

where P is the time series of the concerned signal and mid-span ($z/D = 0$) is used as a reference point. Consider the span-wise correlation of the lift direction first. Figures 13(a) and 13(b) show the span-wise correlation of C_L and Y/D respectively. In the off-resonant case, both the span-wise correlation of C_L (Figure 13(a)) and that of Y/D (Figure 13(b)) vary along the span. However, the span-wise correlation of C_L is fairly constant along the central part of the cylinder and abruptly drops near the ends, while the span-wise correlation of Y/D shows a smooth drop along the cylinder span. This leads to the behavior that the correlation of the force and the displacement shows smooth drop at the central part and becomes relatively constant near the ends (Figure 12(a)). At resonance, however, the span-wise correlation of C_L and Y/D are fairly constant along the span and both are close to unity. Along with correlation between C_L and Y/D (Figure 12(a)), these results suggest that the lift force and the Y/D displacement of the cylinder synchronize along the cylinder span in the resonance case.

In the drag direction, the span-wise correlation of C_D and the corresponding X/D is shown in Figures 14(a) and 14(b) respectively. The behavior in the resonant and the

off-resonant case is similar and differ from those shown in Figure 13. This can be attributed to the fact that the fluid force and cylinder vibration in the drag direction are not synchronized even in the resonant case. It can be seen that while the span-wise correlation of C_D is constant and close to unity, that of X/D shows span-wise variation. This indicates that at different cross-section of the cylinder, the fluid force results in both different magnitude and different phase of the cylinder response. This behavior is similar to that in the lift direction in the off-resonant case where synchronization does not occur either. Therefore, a significant result of synchronization is that not only the fluid force and the corresponding cylinder vibration are correlated, the fluid force and the cylinder vibration are also correlated along the span.

6. CONCLUSIONS

An attempt has been made to couple the Euler–Bernoulli beam model and the Navier–Stokes equations to study the flow-induced vibration of an elastic, finite-span cylinder with fixed ends. The results are compared with experimental measurements obtained under essentially identical conditions and the calculations using a discrete-parameter (2-d.o.f.) structural model. Differences between these results are examined and a correction formula is proposed to render the 2-d.o.f. model results consistent with the present predictions.

Two experimental cases are simulated; they are the resonant and the off-resonant case. The span-wise vibration shape of the cylinder in the lift direction, predicted by the present method, agree rather well with the experimental results. The statistics and the frequency spectra of the cylinder vibration at mid-span are then compared in detail, where 2-d.o.f. model results are also available. The present method and the 2-d.o.f. model give similar predictions of the magnitude and the dominant frequencies of the fluid forces; however, the present method predicts larger values of vibration magnitude than the 2-d.o.f. model. This is shown to be reasonable by a theoretical comparison of the two models. Both models also give similar predictions of natural frequency and damping ratio of the first vibration mode of the combined fluid–cylinder system, and the present method gives the predictions of the third vibration mode as well. It is shown that provided the magnitude and the dominant frequency of the fluid force are not much affected by the fluid–structure interaction, the span-wise vibration can be estimated from the 2-d.o.f. result. A formula has been derived for such a correction.

The fluid–structure interaction effect is demonstrated through the analysis of the calculated fluid forces, cylinder vibrations and the correlation data between them. It is found that the feedback of the cylinder vibration affects its phase relation with the fluid force rather than its magnitude and dominant frequency. This suggests that the main effect of the fluid–structure interaction is on the phase relationship. When the fluid force and the cylinder vibration are in resonance, they are synchronized along the cylinder span, and the fluid force and the cylinder vibration are also correlated along the span. For the off-resonant case, the fluid force has different influence on both the magnitude and the phase of the corresponding cylinder vibration along the span.

ACKNOWLEDGMENTS

Funding support from the The Hong Kong Polytechnic University under Grant No. G-V396 and the Research Grants Council of the Government of the HKSAR under Grant Nos. PolyU5159/97E and PolyU5128/98E are gratefully acknowledged.

REFERENCES

1. C. H. K. WILLIAMSON and A. ROSHKO 1988 *Journal of Fluids and Structures* **2**, 355–381. Vortex formation in the wake of an oscillating cylinder.
2. O. M. GRIFFIN and M. S. HALL 1991 *Transactions of the American Society of Mechanical Engineers, Journal of Fluids Engineering* **113**, 526–534. Review-vortex shedding lock-on and flow control in bluff body wakes.
3. R. GOPALKRISHNAN, M. S. TRIANTAFYLLOU, G. S. TRIANTAFYLLOU and D. BARRETT 1994 *Journal of Fluid Mechanics* **274**, 1–21. Active vorticity control in a shear flow using a flapping foil.
4. P. W. BEARMAN 1984 *Annual Review of Fluid Mechanics* **16**, 195–222. Vortex shedding from oscillating bluff bodies.
5. O. M. GRIFFIN, R. A. SKOP and G. H. KOOPMANN 1973 *Journal of Sound and Vibration* **31**, 235–249. The vortex-excited resonant vibrations of circular cylinders.
6. O. M. GRIFFIN and G. H. KOOPMANN 1977 *Journal of Sound and Vibration* **54**, 435–448. The vortex-excited lift and reaction forces on resonantly vibrating cylinders.
7. T. SARPKAYA 1995 *Journal of Offshore Mechanics and Artic Engineering* **117**, 232–238. Hydrodynamic damping, flow-induced oscillations, and biharmonic response.
8. T. SARPKAYA 1979 *Transactions of the American Society of Mechanical Engineers, Journal of Applied Mechanics* **46**, 241–258. Vortex-induced oscillations—a selective review.
9. G. PARKINSON 1989 *Progress in Aerospace Science* **26**, 169–224. Phenomena and modeling of flow-induced vibrations of bluff bodies.
10. O. M. GRIFFIN 1980 *Transactions of the American Society of Mechanical Engineers, Journal of Pressure Vessel Technology* **102**, 158–166. Vortex-excited cross-flow vibrations of a single cylindrical tube.
11. S. SZEPESSY and P. W. BEARMAN 1992 *Journal of Fluid Mechanics* **234**, 191–217. Aspect ratio and end plate effects on vortex shedding from a circular cylinder.
12. D. BRIKA and A. LANEVILLE 1984 *Journal of Fluid Mechanics* **250**, 481–508. Vortex-induced vibrations of a long flexible circular cylinder.
13. A. KHALAK and C. H. K. WILLIAMSON 1996 *Journal of Fluids and Structures* **10**, 455–472. Dynamics of a hydroelastic cylinder with very low mass and damping.
14. G. S. WEST and C. J. APELT 1997 *Journal of Fluids and Structures* **11**, 135–158. Fluctuating lift and drag forces on finite lengths of a circular cylinder in the subcritical Reynolds number range.
15. R. M. C. SO, Y. ZHOU and M. H. LIU 2000 *Experiments in Fluids* **29**, 130–144. Free vibrations of an elastic cylinder in a cross flow and their effects on the near wake.
16. R. CHILUKURI 1987 *Transactions of the American Society of Mechanical Engineers, Journal of Fluids Engineering* **109**, 166–171. Incompressible laminar flow past a transversely vibrating cylinder.
17. R. A. SKOP and O. M. GRIFFIN 1973 *Journal of Sound and Vibration* **27**, 225–233. A model for the vortex-excited resonant response of bluff cylinders.
18. W. D. IWAN and R. D. BLEVINS 1974 *Transactions of the American Society of Mechanical Engineers, Journal of Applied Mechanics* **41**, 581–586. A model for vortex induced oscillation of structures.
19. C. Y. ZHOU, R. M. C. SO and K. LAM 1999 *Journal of Fluids and Structures* **13**, 165–189. Vortex-induced vibrations of an elastic circular cylinder.
20. R. M. C. SO, Y. LIU, S. T. CHAN and K. LAM 2000 *Journal of Fluids and Structures*. Numerical studies of a freely vibrating cylinder in a cross flow (accepted).
21. K. M. LIEW and K. C. HUNG 1995 *International Journal of Solids and Structures* **32**, 3499–3513. Three-dimensional vibratory characteristics of solid cylinders and some remarks on simplified beam theories.
22. K. M. LIEW, K. C. HUNG and M. K. LIM 1995 *Transactions of the American Society of Mechanical Engineers, Journal of Applied Mechanics* **62**, 718–724. Vibration of stress-free hollow cylinders of arbitrary cross section.
23. T. Y. NG, K. Y. LAM and J. N. REDDY 1998 *Journal of Sound and Vibration* **214**, 513–529. Parametric resonance of a rotating cylindrical shell subjected to periodic axial loads.
24. R. A. SKOP and O. M. GRIFFIN 1975 *Journal of Sound and Vibration* **41**, 263–274. On a theory for the vortex-excited oscillations of flexible cylindrical structures.
25. R. A. SKOP and S. BALASUBRAMANIAN 1997 *Journal of Fluids and Structures* **11**, 395–412. A new twist on an old model for vortex-excited vibrations.

26. V. MUKHOPADHYAY and J. DUGUNDJI 1976 *Journal of Sound and Vibration* **45**, 329–339. Wind excited vibration of a square section cantilever beam in smooth flow.
27. D. J. NEWMAN and G. KARNIADAKIS 1997 *Journal of Fluid Mechanics* **344**, 95–136. A direct numerical simulation study of flow past a freely vibrating cable.
28. M. S. BLOOR 1964 *Journal of Fluid Mechanics* **19**, 290–304. The transition to turbulence in the wake of a circular cylinder.
29. C. Y. ZHOU, R. M. C. SO and M. P. MIGNOLET 2000 *Journal of Fluids and Structures*, **14**, 303–322. Fluid damping of an elastic cylinder in a cross flow.
30. C. EVANGELINOS & G. E. KARNIADAKIS 1999 *Journal of Fluid Mechanics* **400**, 91–124. Dynamics and flow structures in the turbulent wake of rigid and flexible cylinders subject to vortex-induced vibrations.
31. C. EVANGELINOS, D. LUCOR & G. E. KARNIADAKIS 2000 *Journal of Fluids and Structures* **14**, 429–440. DNS-derived force distribution on flexible cylinders subject to vortex-induced vibration.
32. J. H. GERRARD 1961 *Journal of Fluid Mechanics* **11**, 244–265. An experimental investigation of the oscillating lift and drag of a circular cylinder shedding turbulent vortices.
33. R. E. D. BISHOP & A. Y. HASSAN 1964 *Proceedings of the Royal Society* **A277**, 51–75. The lift and drag forces on a circular cylinder in a flowing fluid.
34. A. RICHTER, & E. NAUDASCHER 1976 *Journal of Fluid Mechanics* **78**, 561–576. Fluctuating forces on a rigid circular cylinder in a confined flow.
35. R. M. C. SO and S. D. SAVKAR 1981 *Journal of Fluid Mechanics* **105**, 397–425. Buffeting forces on rigid circular cylinders in cross flows.
36. I. JADIC, R. M. C. SO and M. P. MIGNOLET 1998 *Journal of Fluids and Structures* **12**, 631–654. Analysis of fluid–structures interactions using a time marching technique.
37. P. A. MENDES and F. A. BRANCO 1999 *International Journal for Numerical Methods in Fluids* **30**, 897–919. Analysis of fluid–structure interaction by an arbitrary Lagrangian–Eulerian finite element formulation.
38. J. R. MOONEY and A. N. STOKES 1998 *Applied Mathematical Modeling* **22**, 949–962. Time-varying MHD flows with free surfaces.
39. R. GLOWINSKI and O. PIRONNEAU 1992 *Annual Review of Fluid Mechanics* **24**, 167–204. Finite element methods for Navier–Stokes equations.
40. L. MEIROVITCH 1997 *Principles and Techniques of Vibrations*. Englewood Cliffs, NJ: Prentice-Hall Inc, International Edition.
41. M. P. MIGNOLET and J. R. RED-HORSE 1994 *Proceedings of the 35th Structures, Structural Dynamics, and Materials Conference, AIAA/ASME, Hilton Head, South Carolina, April* 18–20, 1628–1637. ARMAX identification of vibrating structures: model and model order estimation.